# Mechanisms of Water Interaction with Pore Systems of Hydrochar and Pyrochar from Poplar Forestry Waste

Conte, Pellegrino ; Hanke, Ulrich Michael ; Marsala, Valentina ; Cimò, Giulia ; Alonzo, Giuseppe ; Glaser, Bruno

DOI: https://doi.org/10.1021/jf5010034

JOURNAL OF AGRICULTURAL AND FOOD CHEMISTRY

Article

# MECHANISMS OF WATER INTERACTION WITH PORE SYSTEMS OF HYDROCHAR AND PYROCHAR FROM POPLAR FORESTRY WASTE

Pellegrino Conte, Ulrich M. Hanke, Valentina Marsala, Giulia Cimò, Giuseppe Alonzo, and Bruno Glaser

*J. Agric. Food Chem.*, **Just Accepted Manuscript** • Publication Date (Web): 09 May 2014

# MECHANISMS OF WATER INTERACTION WITH PORE SYSTEMS OF HYDROCHAR AND PYROCHAR FROM POPLAR FORESTRY WASTE

Pellegrino Conte[1*], Ulrich M. Hanke[2,†], Valentina Marsala[1], Giulia Cimò[1], Giuseppe Alonzo[1], Bruno Glaser[2]

1. Dipartimento di Scienze Agrarie e Forestali, Università degli Studi di Palermo v.le delle Scienze edificio 4, 90128 Palermo – Italy
2. Soil Biogeochemistry, Martin-Luther-University Halle-Wittenberg, von-Seckendorff-Platz 3, 06120 Halle – Germany

**Running title**: Water dynamics on hydrochar and pyrochar surfaces

*. **Corresponding and contact author**: Pellegrino Conte; E-Mail: pellegrino.conte@unipa.it; Ph.: 003909123864673; Fax: 0039091484035

†. Present address: Soil Science and Biogeochemistry, University of Zurich, Winterthurerstrasse 190, 8057 Zürich - Switzerland

**Abstract**

The aim of this paper was to understand the water-surface interactions of two chars obtained by gasification (pyrochar) and hydrothermal carbonization (hydrochar) of a poplar biomass. The two samples revealed different chemical composition as evidenced by solid state $^{13}C$ NMR spectroscopy. In fact, hydrochar resulted in a lignin-like material still containing oxygenated functionalities. Pyrochar was a polyaromatic system where no hetero-nuclei were detected. After saturating with water, hydrochar and pyrochar were analyzed by fast field cycling (FFC) NMR relaxometry. Results showed that water movement in hydrochar was mainly confined in very small pores. Conversely, water movement in pyrochar led to the conclusion that a larger number of transitional and very large pores were present. These results were confirmed by porosity evaluation derived from gas adsorption. Variable temperature FFC NMR experiments confirmed slow motion regime due to a preferential diffusion of water on the solid surface. Conversely, the larger number of large pores in pyrochar allowed slow movement only up to 50 °C. As temperature was raised to 80 °C, water interactions with the pore surface became weaker, thereby allowing a 3D water exchange with the bulk liquid. This paper has shown that pore size distribution was more important than chemical composition in affecting water movement in two chemically different charred systems.

**Keywords**: fast field cycling NMR; relaxometry; hydrochar; pyrochar; biochar; water dynamics

## Introduction

Recent scientific research addressed applications of charred biomasses for environmental remediation and agricultural productivity.[1-3] In fact, use of charred biomasses has been suggested as a solution to counteract enhancement of atmospheric carbon dioxide,[4,5] for water and soil remediation[6-8] and for improvement of soil fertility.[2] In particular, char applied deliberately to soils, which Lehmann and Joseph [9] have recently classified as biochar, can modify soil pH,[10] increase soil draining capacity,[11] improve cation exchange capacity,[12] mitigate salt-induced stresses[13] and interact with soil fertilizers,[14] thereby favoring microbial activity[15] and plant growth.[14,16]

Notwithstanding the positive effects of biochar applications to soils, some authors have warned about its potential detrimental impacts on environment. For example, increase of $CO_2$ emissions to atmosphere, due to enhancement of soil C mineralization rate after biochar applications to soils, has been described.[17] Also plant growth inhibition due to temporary high pH values, presence of volatile matter (i.e. tars, resins, and other short-lived substances that remain on the biochar surface immediately after production), and nutrient imbalances associated with the use of fresh biochars have been reported.[18,19]

Certainly, functions of chars in the environment depend on their physico-chemical properties which, in turn, are most affected by feedstock type, pyrolysis conditions, and duration of charring.[3,9-11,20-25] As an example, aromatic condensation in chars increases with increasing heating temperature.[20,24] Moreover, plant species with many large diameter cells in the stem tissues can lead towards chars containing larger amounts of macro pores.[9] Macro pores in biochar applied to soils may enhance soil draining properties and capacity to retain large molecules such as phenolic compounds.[11] On the other hand, micro pores may adsorb water with high capillary forces so that it is not available for most plants. For this reason, understanding char physical and chemical processes at the char surface is very crucial in order to address its agronomical and environmental uses and allow meaningful pre-application quality assessments.

Nuclear magnetic resonance (NMR) techniques are usually applied to monitor char characteristics.[10,20,22,24,26] In particular, low field NMR relaxometry with fast field cycling setup (FFC NMR) can be used to study the dynamics of water in chars in order to retrieve information about the possible molecular mechanisms through which water (and therefore micro and macro nutrients) can be drained in char-amended soils.

In previous studies, FFC NMR relaxometry was applied to differentiate among pore size distribution on the surface of chars obtained by an industrial gasification procedure[10] and to recognize the nature of the interactions between water and char surfaces.[26] These studies were conducted only on chemically identical chars. However, no information is available on the dynamics of water in chars having different chemical composition. For this reason, in the present study, we selected a hydrochar already analyzed by Wiedner et al.[24] and a pyrochar studied in De Pasquale et al.[10] and Conte et al.[26], both obtained by the same biomass feedstock, with the aim to investigate the role played by chemical characteristics on water dynamics within the pore system of the chars.

## Materials and Methods

**Feedstock**. The hydrochar and pyrochar samples were prepared by using poplar (*Populus spp.* L.) wood chips which were obtained from dedicated short rotation forest in the Po Valley (Gadesco Pieve Delmona, $45°10^{I}13^{II}$ N, $10°06^{I}01^{II}$ E). The age of the forest at the time of harvest was five years. The characteristics of the biomass were already described in De Pasquale et al.[10]

**Pyrochar and hydrochar preparation**. Pyrochar was produced by using an industrial gasifier at the temperature of 1200 °C. All the details about the gasifier and the pyrolitic conditions have been already reported in De Pasquale et al.[10] Hydrochar was obtained in a b.coal 2.0 reactor from Artec Biotechnology GmbH (Bad Königshofen, Germany) at 230 °C and 40 bar. Details about the procedure have been reported already in Wiedner et al.[24] Both pyrochar and hydrochar samples

were 2 mm sieved with a stainless steel sieve and dried overnight in an oven set at 105 °C before each NMR analysis.

**Specific surface area measurement**. Samples were first dried at 200 °C for 4.5 hours, then stored in a desiccator. In order to retrieve the specific surface area by applying the Brunauer–Emmett–Teller (BET) 5-points method, samples were degassed with $N_2$ at 200 °C for another hour and then measured in liquid $N_2$ (Quantachrome NOVA 4200 calibrated with BAM-PM-104) following DIN ISO 9277:2003-05. All measurements were done in triplicate. Specific surface area of the pyrochar and the hydrochars were 54.6 ± 0.2 $m^2g^{-1}$ and 129 ± 2 $m^2g^{-1}$, respectively.

The poplar pyrochar surface area measured in this study was smaller than that already reported in De Pasquale et al.[10] (i.e. 98 ± 6 $m^2g^{-1}$). The difference can be explained by the different sample preparation used in De Pasquale et al.[10] prior to BET analysis. In fact, the BET investigations reported in De Pasquale et al.[10] have been conducted on agate-mortar-ground samples. Pyrochar grinding reduces particle sizes, thereby increasing surface area values.

**Evaluation of pore size distribution from the specific surface area measurements.** The non-local density functional theory (NLDFT) equilibration model[27] was applied to elaborate the isotherms (35 adsorption and 30 desorption points) of nitrogen adsorption experiments in order to achieve pore size distributions. Assumption of $N_2$ at -196 °C on carbon (slit-pore) was used. The cumulative pore volumes and surface areas for the micro pore class (i.e. < 2 nm, according to IUPAC classification) retrieved by NLDFT model were 16.3x$10^{-3}$ $cm^3 \cdot g^{-1}$ and 29.4 $m^2 \cdot g^{-1}$ for pyrochar, while they resulted 50.9 x$10^{-3}$ $cm^3 \cdot g^{-1}$ and 93.3 $m^2 \cdot g^{-1}$ for hydrochar. NLDFT surface area and pore volume for hydrochar resulted around three times higher than those for pyrochar, thereby evidencing that the amount of pores in the former sample was larger than in the latter one. In particular the Surface/Volume (S/V) ratios from NLDFT elaborations were $(S/V)_{pyrochar}$=1.80 x $10^9$ $m^{-1}$ and $(S/V)_{hydrochar}$=1.83 x $10^9$ $m^{-1}$.

**CP-TOSS $^{13}$C NMR spectra**. Cross polarization magic angle spinning (CPMAS) $^{13}$C NMR measurements were performed on a Bruker Avance-II 400 spectrometer (Bruker Biospin, Milan,

Italy) operating at 100.6 MHz on carbon-13 and equipped with a 4 mm standard bore solid state probe. Samples were packed into 4 mm zirconia rotors with Kel-F caps and the rotor spin rate was set at 5000 ± 2 Hz. A spectral width of 25252.52 Hz centered at 10061.78 Hz, an optimum contact time of 1 ms chosen after evaluation of variable contact time experiments, a recycle delay of 20 s, 2 k data points over an acquisition time of 35 ms were used. The spectra were acquired with the total suppression side bands (TOSS) sequence with a 50% RAMP in order to prevent artifacts in the spectra interpretation. A 4.1 μs $^{1}$H 90° pulse with an attenuation level of -2.4 dB was applied. Spectra acquisition was achieved with Bruker Topspin® 2.0. Data processing was done with MestRe-C software (Version 4.9.9.9, Mestrelab Research, Santiago de Compostela, Spain). The free induction decays (FIDs) were transformed by applying first a 2 k zero filling, then a line broadening of 100 Hz and finally an automatic baseline correction with a 3rd order polynomial and Bernstein algorithm.

**Fast field cycling (FFC) NMR relaxometry**. The 2 mm sieved and dried poplar pyrochar and hydrochar samples have been prepared as slurry for fast field cycling (FFC) NMR relaxometry investigations according to the procedure reported in Dunn et al.[28] The background theory of FFC NMR relaxometry has been already described in De Pasquale et al.[10] Moreover, more general environmental applications of FFC NMR relaxometry can be found in Conte and Alonzo.[29]

$^{1}$H nuclear magnetic resonance dispersion profiles (i.e. relaxation rates $R_1$ or $1/T_1$ vs. proton Larmor frequencies) were acquired on a Stelar Spinmaster FFC2000 Relaxometer (Stelar s.r.l., Mede, PV–Italy) at temperatures of 25 °C, 50 °C and 80 °C. The proton spins were polarized at a $B_{POL}$ corresponding to the proton Larmor frequency ($\omega_L$) of 24 MHz for a $T_{POL}$ corresponding to about five times the $T_1$ estimated at this frequency. After each $B_{POL}$ application, the magnetic field intensity (indicated as $B_{RLX}$) was systematically changed in the proton Larmor frequency $\omega_L$ comprised in the range 0.01-40 MHz. The period $\tau$, during which $B_{RLX}$ was applied, has been varied on 32 logarithmic spaced time sets, each of them adjusted at every relaxation field in order to

optimize the sampling of the decay/recovery curves. Free induction decays (FID) were recorded following a single $^1$H 90° pulse applied at $B_{ACQ}$ corresponding to the proton Larmor frequency of 16 MHz. A time domain of 100 μs sampled with 512 points was applied. Field switching time was 3 ms, while spectrometer dead time was 15 μs. For all experiments, a recycle delay of 12 s was used. The NP sequence was applied when the relaxation magnetic fields were in the range of the proton Larmor frequencies between 40.0 and 9.0 MHz. The PP sequence was applied in the proton Larmor frequencies $B_{RLX}$ range of 9.0-0.01 MHz.[30]

**FFC NMR data processing**. $R_1$ values were achieved by interpolating the $^1$H magnetization decay/recovery curves at each $B_{RLX}$ value (i.e. $^1$H signal intensity versus τ) with the stretched exponential function (also known as Kohlrausch-Williams-Watts function) reported in equation [1] after exportation of the experimental data to OriginPro 7.5 SR6 (Version 7.5885, OriginLab Corporation, Northampton, MA, USA). This equation provided the best fitting with the largest coefficients of determination ($R^2 > 0.998$). The choice of this function was due to the large sample heterogeneity resulting in a multi-exponential behavior of the decay/recovery curves.[29,31] This approach has the advantage that it is able to handle a wide range of behaviors within a single model. For this reason, assumptions about the number of exponentials to be used in modeling NMRD data are not necessary.

$$I(\tau) = I_0 \exp\left[-(\tau/T_1)^k\right] \qquad [1].$$

In equation [1], I(τ) is the $^1$H signal intensity at each fixed $B_{RLX}$, $I_0$ is the $^1$H signal intensity at the thermal equilibrium, $T_1$ is the average proton spin lattice relaxation time and *k* is a heterogeneity parameter related to the stretching of the decay process. This function can be considered as a superposition of exponential contributions, thereby describing the likely physical picture of some distribution in $T_1$.

Relaxation data at the proton Larmor frequency of 40 MHz were evaluated by the inverse Laplace transformation through application of the UPEN algorithm (Alma Mater Studiorum – Università di

Bologna, Italy)[32,33] with the aim to obtain the $T_1$ distributions at such magnetic field and, therefore, information on pore distribution, and grain size. The choice of UPEN analyses only at 40 MHz was due to the larger NMR sensitivity at this frequency as compared to the other proton Larmor frequencies.[30]

## Results and Discussion

**Hydrochar and pyrochar chemical composition by CP-TOSS $^{13}$C NMR spectroscopy**. The cross polarization magic angle spinning with total suppression of side bands $^{13}$C NMR spectra of the two samples studied here, showed the more complex nature of hydrochar as compared to pyrochar (Figure 1). In particular, two main regions can be recognized in the hydrochar spectrum (Figure 1A). The first chemical shift interval between 0 – 80 ppm contains individual signals at 16, 30, 48, 56 and 72 ppm (Figure 1A). The first signal at 16 ppm can be attributed to methyl groups of terminating alkyl chains; the second one at 30 ppm is due to methylene groups in alkyl chains, whereas the signal at 48 ppm can be assigned to branched alkyl carbons; the signal at 56 ppm is assignable to methoxyl groups in lignin-like structures and that at 72 ppm is due to carbons C2, C3, C5 in the residual cellulose moiety from the poplar biomass.[24,34]

The second spectral region in Figure 1A occurred in the chemical shift interval between 90 – 160 ppm. The main signals recognized in this region are broad bands centered at 106, 115, 133 and 147 ppm. The signal at 106 ppm can be assigned to C1 in residual cellulose; that at 115 ppm is due to C5 in guaiacyl (G) and C3 and C6 in *p*-hydroxyphenyl groups; the signal at 133 ppm is due to the aromatic C–5/C–5' in etherified 5–5 G units; finally the signal at 147 ppm is assigned to C3 and C4 in etherified guaiacyl units.[24,34]

The spectrum reported in Figure 1B reveals only one broad band at 126 ppm which can be assigned to polyaromatic systems.[10] The differences in the chemical composition of poplar hydrochar and pyrochar samples (Figure 1) can be explained by the different types of reactions occurring as either hydrothermal carbonization[24] or gasification[10] are applied. The hydrothermal carbonization used in

this study consisted of a thermal degradation of the water-suspended-biomass at high pressure and 230 °C by applying citric acid as catalyst.[24] During this process, carbohydrates in poplar biomass have been gradually transformed to aromatic and aliphatic structures, thereby providing a lignin-like material. However, the presence of signals at 56, 72, 106, 133 and 147 ppm (Figure 1A) indicates that the hydrothermal carbonization produced a carbonaceous material still containing oxygenated functionalities, but almost no poly-condensed aromatic moieties as outlined in Wiedner et al.[24]

The sole aromatic signal in the CP-TOSS $^{13}C$ NMR spectrum of the poplar pyrochar (Figure 1B) is due to the diamagnetic currents produced by delocalized π-electrons in extended aromatic structures or graphite-like micro-crystallites which are generated by the high temperature condensations as biomass feedstock is subjected to gasification.[10]

**Effect of pore size on $^{1}H$ NMR $T_1$ distributions**. The 2 mm sieved poplar hydrochar and pyrochar samples were saturated with water and the slurry analyzed by fast field cycling NMR relaxometry as indicated in Materials and Methods. Figure 2 reports the distributions of the longitudinal relaxation times ($T_1$), also referred to as relaxograms, at the proton Larmor frequency of 40 MHz and three temperatures (25, 50 and 80 °C) as obtained by applying the inverse Laplace transformation of the relaxation data through the UPEN algorithm (see Materials and Methods).

Proton longitudinal relaxation times of water in porous media are affected by the collisions between the liquid state molecules and the walls of the porous boundaries.[35] In particular, longitudinal relaxation is dominated by the presence of a strong relaxation sink at the pore surface which is imputable to the temporary adsorption of water on the solid surface.[36] Temporary adsorption can be achieved by formation of weak un-conventional hydrogen bonds on the surface of pyrogenic char systems as already outlined in Conte et al.[26] and Conte and Alonzo.[29] However, as surficial polar groups are present, the weak un-conventional H-bonds may turn towards stronger conventional ones which may hook water molecules more strongly on the char surface. The effectiveness of the aforementioned relaxation sink depends on the ratio between the pore surface and the pore volume

as well as on the diffusion rate across the pore.[37] In fact, space restriction in small sized pores do not allow fast molecular mobility. As this condition occurs, $^{1}H$-$^{1}H$ dipolar interactions result very efficient. Shorter relaxation times are, hence, retrieved.[35,37,38] Conversely, as pore size enlarges, molecular mobility increases and strength of dipolar interactions weaken. For this reason, longer relaxation times are expected.[35,37,38] As the number and size of the various pores present in a material is heterogeneous, water must diffuse through the differently sized pores, thereby providing a wide ensemble of longitudinal relaxation times which appear continuously distributed. The lowest limit of such ensemble (the shortest $T_1$ value) is due to water moving into the smallest pores, whereas the highest limit (the longest $T_1$ value) is attributed to water moving into the largest pores. All $T_1$ values between the two limits are due to the dynamics of water inside pores having sizes lying between the two extremes.[29] According to the aforementioned mechanism, the differences observed at the same temperatures between the $T_1$ distributions reported in Figure 2 can be attributed to different pore size distribution present in the hydrochar and pyrochar samples. In particular, a homogeneous distribution of small sized pores can be recognized in hydrochar rather in pyrochar. The latter, in turn, is made by a less homogeneous distribution of pores which are averagely larger than in hydrochar. In fact, all the hydrochar relaxograms showed a maximum centered at a $T_1$ value of around 100 ms regardless of the temperature used during the experiments (Figure 2A). Conversely, the relaxograms acquired for the water-saturated pyrochar span a larger interval of $T_1$ values (Figure 2B). Here a maximum at 100 ms independent of the applied temperature (similarly to the water-saturated hydrochar sample) can be observed. Moreover, a second maximum centered at 479, 340 and 290 ms retrieved at 25 °C, 50 °C and 80 °C, respectively, is also observed (Figure 2B). A wide distribution of $T_1$ values is included among the two longitudinal relaxation time limits in Figure 2B. We can identify water molecules relaxing at 100 ms in both carbonaceous samples as those restricted in the smallest sized pores; water molecules generating the maxima at 479 ms at 25 °C, 340 ms at 50 °C and 290 ms at 80 °C as those

tumbling in the largest pores; finally, water molecules relaxing in the intervals 100 – 479 ms at 25 °C, 100 – 340 ms at 50 °C and 100 – 290 ms at 80 °C as those occluded in transitional pores.

The aforementioned findings are supported by BET and NLDFT elaborations as reported in Materials and Methods. In fact, specific surface areas were 54.6 ± 0.2 $m^2g^{-1}$ and 129 ± 2 $m^2g^{-1}$ for pyrochar and hydrochar respectively, thereby suggesting a larger volume of pores in the former than in the latter sample. On the other hand, NLDFT elaborations of isotherms obtained from nitrogen adsorption provided S/V ratios in the order $(S/V)_{pyrochar} < (S/V)_{hydrochar}$ (see Material and Methods). It is well known that the longitudinal relaxation rate ($1/T_1$) is directly proportional to the S/V ratio[39] or, by considering the reciprocal:

$$T_1 \propto \frac{V}{S}$$

Since $(S/V)_{pyrochar} < (S/V)_{hydrochar}$, it comes that $(V/S)_{pyrochar} > (V/S)_{hydrochar}$ and it is expected that the $T_1$ values for pyrochar must be longer than for hydrochar. The latter expectation has been evidenced in the experimental results showed in Figure 2 and discussed above.

It is interesting to note that the relaxogram reported in De Pasquale et al.[10] was obtained for the same pyrochar used in the present study. However, the $T_1$ distribution in De Pasquale et al.[10] revealed a larger pore size homogeneity than the relaxogram reported here in Figure 2B. This difference can be explained by considering that samples were prepared differently prior to the analysis. In fact, in the present study, we sieved the poplar pyrochar < 2 mm, whereas in De Pasquale et al.[10] the sample has been grounded. As already outlined in Materials and Methods, sample grinding reduces pore size, thereby allowing larger surface area and more homogeneous pore size distribution.

**Effect of temperature on $^1$H NMR $T_1$ distributions**. Longitudinal relaxation times are not only dependent on the pore size distribution, as outlined in the previous paragraph, but also on temperature variations.[29] In fact, it is well recognized that temperature increments accelerate molecular motions, thereby weakening the $^1$H-$^1$H dipolar interactions responsible for the

longitudinal relaxation of a liquid moving on the surface of porous materials.[40] When this condition occurs, an increase of $T_1$ values is expected since a longer time is needed for proton spin lattice relaxation. However, it has been already shown that water retained in charred materials behaves diametrically, thereby suggesting that water dynamics is subjected to a slow motion regime.[26] The latter is achieved when water molecules are hooked to the char surface via weak hydrogen bonds that may arise by the overlay of the electron-deficient orbitals of protons in water and the electron-rich orbitals in the organic and inorganic components of the charred system.[26] As temperature increases, the weak interactions, which allow water adhesion to the pore walls, oppose to the 3D exchange with the bulk water (i.e. the replacement of water molecules hooked to the char surface with those appertaining to the bulk liquid).[40] For this reason, water preferentially diffuses faster within the channels connecting pores between each other through a 2D motion (i.e. the diffusion of water molecules within the channels connecting either different surface pores or char surface with the interior part of the same material).[26,40] Due to the 2D surface diffusion just described, water collision frequency with pore walls increases with temperature, thereby allowing an average residence time on pore walls longer than that retrieved at lower temperatures. Because of this, shorter time for protons to relax is needed and lower $T_1$ values are achieved.[40] As a consequence, relaxograms, such as those in Figure 2, shrink as temperature is increased. Moreover, it must be added that the larger the pore size, the more pronounced is the reduction of the relaxogram width and the reduction of the $T_1$ maxima. In fact, upon temperature increasing, water collision frequency in larger pores becomes higher than in the more spatially restricted ones. Because of this, the average time spent by water molecules on pore walls is higher in the transitional and the largest pores than in the smallest pores. The latter is the reason why the reduction of relaxogram widths is less pronounced in Figure 2A than in Figure 2B. Moreover, the same mechanism explains why the maximum at 100 ms due to water in the smallest pores either in hydrochar or in pyrochar is unaffected by temperature changes, whereas the $T_1$ maxima due to water in larger sized pores ($T_1$ >100 ms) shift towards shorter values.

294 **NMRD profiles**. Figure 3 shows the nuclear magnetic resonance dispersion (NMRD) profiles (i.e.
295 $R_1=1/T_1$ values vs $\omega_L$) at 25, 50 and 80 °C for the water-saturated poplar hydrochar and pyrochar
296 samples investigated here. In particular, the NMRD profiles of the former sample are all placed at
297 faster longitudinal relaxation rates (Figure 3A) as compared to the NMRD profiles of the latter
298 sample (Figure 3B). This is due to the differences in the surface areas between the two porous
299 materials. In fact, $SSA_{hydrochar}$ was larger than $SSA_{pyrochar}$ (see above). The larger the surface area
300 value, the smaller is the size of the pores. Restriction of water in small pores leads to stronger $^1H$-$^1H$
301 dipolar interactions which, in turn, are the cause for the very efficient proton longitudinal relaxation
302 in hydrochar (i.e. faster $R_1$ values) compared to pyrochar.[41]
303 It is worth to note that all the NMRD profiles in Figure 3A are translated towards faster $R_1$ values in
304 the whole range of proton Larmor frequencies as temperature was increased. This behavior accords
305 with that already described in Conte et al.[26], thereby confirming the slow motion regime also
306 outlined in the previous paragraph. However, Conte et al.[26] reported that the slow motion regime on
307 the surface of char systems is due to non-conventional H-bonds arising by the overlay between the
308 electron-deficient orbitals of protons in water and the electron-rich orbitals of the aromatic organic
309 centers in the charred material. In the present study, we have reported that hydrothermal
310 degradation did not remove all the oxygen-containing functionalities (see above). For this reason,
311 we cannot exclude participation of the more traditional O-H···O bonds in the slow motion regime
312 observed for the hydrochar sample.
313 Figure 3B reveals that the NMRD profiles acquired for the pyrochar sample behaved similarly to
314 the hydrochar only up to 50 °C. Conversely, an anomalous trend was observed at 80 °C. In fact, a
315 slight increment of the $R_1$ values was retrieved between 40 and 10 MHz as temperature was
316 switched from 50 to 80 °C. Then the 80 °C NMRD profile crossed the one acquired at 50 °C as $\omega_L$
317 was set to 10 MHz and that retrieved at 25 °C as $\omega_L$ was switched to 0.2 MHz (Figure 4B). The H-
318 bond-mediated slow motion regime can explain the NMRD behavior up to 50 °C observed for the

pyrochar sample (Figure 3B). However, as temperature is raised up to 80 °C, a chemical exchange with the bulk phase must be considered in order to account for the anomalous behavior reported in Figure 3B.[40]

The interesting feature that the temperature dependence of water dynamics in hydrochar is opposite to that observed in pyrochar can only be explained by considering the different pore size distribution in the two carbonaceous samples. In fact, as outlined above, the average pore size in hydrochar is smaller than in pyrochar. Water molecules are more tightly trapped in the former than in the latter material. For this reason, water can easily run away towards the bulk liquid from pyrochar rather than from hydrochar surface as temperature was increased up to 80 °C.

The comparison among the temperature dependence of the NMRD profiles in Figure 3 and those in Conte et al.[26] supports the latter hypothesis on the role played by pore size in water exchange with the bulk solution. In fact, the pyrochar analyzed either in the present study or in Conte et al.[26] was obtained by the same gasification process.[10] However, while in Conte et al.[26] the pyrochar was grounded in an agate mortar before NMRD investigations, here we have performed NMRD analyses after having sieved the same material < 2 mm. As a consequence, the surface area of the grounded pyrochar[26] resulted larger than that used in the present study. As already noted above, larger surface area was associated with a more homogeneous pore size distribution made mainly by the smallest pores. Conversely, more inhomogeneous distribution of pore size (with a larger contribution from transitional and larger pores) was identified in the porous charred material having lower surface area. Hence, the more inhomogeneous pore size pyrochar used here revealed the anomalous temperature dependence behavior at 80 °C (Figure 3B) due to the higher amount of larger pores which make the exchange of surface water molecules with the bulk ones easier.

This paper reports about high and low field NMR characterization of the physico-chemical properties of hydrochar and pyrochar samples retrieved by applying either hydrothermal treatment or gasification to poplar forestry wastes. In particular, high field NMR spectroscopy (i.e. CP-TOSS $^{13}C$ NMR) revealed that the thermal treatments produced two chemically different carbonaceous

materials. While poplar hydrochar appeared as a lignin-like material still containing oxygenated functionalities, poplar pyrochar emerged as a polyaromatic system where O-containing groups were not detected.

Notwithstanding the different chemical compositions, the mechanisms of water dynamics on the surface of poplar hydrochar and pyrochar were affected more by their physical characteristics rather than by their chemical peculiarities. In particular, isothermally 40 MHz acquired relaxograms revealed that water motion was more restricted in hydrochar than in pyrochar, thereby suggesting that the former sample included a larger number of small-sized pores than the latter one. On the other hand, the more free motion of water in pyrochar indicated a higher amount of transitional and very large pores.

Variable temperature relaxometry experiments revealed that 2D surface diffusion mechanism was the only force responsible for water motion in hydrochar up to the temperature of 80 °C. Surface diffusion was the predominating motion mechanism of water in pyrochar only up to 50 °C. Conversely, a 3D exchange with the bulk water appeared to interfere with the aforementioned 2D diffusion as temperature was raised up to 80 °C.

The differentiation between the 2D diffusion and the 3D exchange mechanisms was attributed to the different porosity in the charred materials. In fact, water constrained in small pores such as in hydrochar strongly interacts with the solid surfaces. For this reason, its fugacity towards the bulk liquid is inhibited in the whole temperature interval investigated here (25 – 80 °C). On the other hand, the larger pore sizes in poplar pyrochar prevent water exchange with the bulk solution only in a more restricted temperature interval (namely, 25 – 50 °C). As temperature overcomes the limit of 50 °C, water surface interactions become weaker and 3D exchange with the bulk liquid occurs.

Although in the present study the chemical composition of poplar hydrochar and pyrochar appeared of minor importance to the water dynamics, its contribution to the strength of water solid phase interactions is not yet clear. For this reason, more detailed studies on the effect of pore sizes and chemical composition of charred materials on water dynamics are urgently needed.

**Acknowledgments**

The authors are grateful to Centro Grandi Apparecchiature – UniNetLab of Università degli Studi di Palermo (http://www.unipa.it/cga/index.html) for having provided machine time at the high field NMR spectrometer for the acquisition of the CP-TOSS $^{13}C$ NMR spectra.

We appreciate the support of COST action TD1107 (Biochar for sustainable resources management) for the Short-term Scientific Mission (STSM) of Ulrich M. Hanke.

Dr. Alessandro Pozzi (AGT technologies) is acknowledged for providing the pyrochar sample.

**References**

1. Glaser, B.; Haumaier, L.; Guggenberger, G.; Zech, W. The "Terra Petra" phenomenon a model for sustainable agriculture in the humid tropics. *Naturwissenschaften* **2001**, *88* (1), 37-41; DOI: 10.1007/s001140000193.
2. Mao, J. D.; Johnson, R. L.; Lehmann, J.; Olk, D. C.; Neves E. G.; Thomson M. L.; Schmidt-Rohr, K. Abundant and stable char residues in soils: implication for soil fertility and carbon sequestration. *Environ. Sci. Technol.* **2012**, 46, 9571-9576.
3. Mukherjee, A.; Lal, R. Biochar impacts on soil physical properties and greenhouse gas emissions. *Agron.* **2013,** *3* (2), 313-339; DOI: 10.3390/agronomy3020313.
4. Glaser, B.; Lehmann, J.; Zech, W. Ameliorating physical and chemical properties of highly weathered soils in the tropics with charcoal – a review. *Biol. Fert. Soils* **2002**, *35* (4), 219-230; DOI: 10.1007/s00374-002-0466-4.
5. Vanderslice, N. C.; Marrero, T. R. Impact of Bio-Char on Carbon Dioxide in the Atmosphere. In *Proceedings of the 2009 Midwest Section Conference of the American Society for Engineering Education;* available at: http://www.asee.org/papers-and-publications/papers/section-proceedings/midwest/2009

6. Mohan, D.; Rajput, S.; Singh, V. K.; Steele, P. H.; Pittman Jr., C. U. Modeling and evaluation of chromium remediation from water using low cost bio-char, a green adsorbent. *J. Hazard. Mater.* **2011**, *188* (1-3), 319–333; DOI: 10.1016/j.jhazmat.2011.01.127.
7. Beesley L.; Moreno-Jiménez E.; Gomez-Eyles J. L.; Harris E.; Robinson B.; Sizmur T. A review of biochars' potential role in the remediation, revegetation and restoration of contaminated soils. *Environ. Pollut.* **2011**, *159* (12), 3269–3282; DOI: 10.1016/j.envpol.2011.07.023.
8. Zhang, X.; Wang, H.; He, L.; Lu, K.; Sarmah, A.; Li, J.; Bolan, N. S.; Pei, J.; Huang, H. Using biochar for remediation of soils contaminated with heavy metals and organic pollutants. *Environ. Sci. Pollut. R.* **2013**, *20* (12); DOI 10.1007/s11356-013-1659-0.
9. Lehmann, J.; Joseph, S. Biochar for environmental management: an introduction. In *Biochar for environmental management: science and technology;* Lehmann, J.; Joseph, S.; Eds.; Routledge: London U. K. 2009; pp. 448.
10. De Pasquale, C.; Marsala, V.; Berns, A.E.; Valagussa, M.; Pozzi, A.; Alonzo, G.; Conte, P. Fast field cycling NMR relaxometry characterization of biochars obtained from an industrial thermochemical process. *J. Soils Sediments* **2012**, *12* (8), 1211–1221; DOI: 10.1007/s11368-012-0489-x.
11. Warnock, D. D.; Lehmann, J.; Kuyper, T. W.; Rilling, M. C. Mycorrhizal responses to biochar in soil – concepts and mechanisms. *Plant Soil* **2007,** *300* (1-2), 9-20; DOI: 10.1007/s11104-007-9391-5.
12. Liang, B.; Lehmann, J.; Solomon, D.; Kinyangi, J.; Grossman, J.; O'Neill, B.; Skjemstad, J. O.; Thies, J.; Luizão, F. J.; Petersen, J.; Neves, E. G. Black Carbon Increases Cation Exchange Capacity in Soils. *Soil Sci. Soc. Am. J.* **2006**, *70* (5), 1719-1730; DOI:10.2136/sssaj2005.0383.
13. Thomas, S. C.; Frye, S.; Gale, N.; Garmon, M.; Launchbury, R.; Machado, N.; Melamed, S.; Murray, J.; Petroff, A.; Winsborough, C. Biochar mitigates negative effects of salt additions

421 on two herbaceous plant species. *J. Environ. Manage.* **2013**, *129,* 62–68; DOI:
422 10.1016/j.jenvman.2013.05.057.
423 14. Chan, K. Y.; Van Zwieten, L.; Meszaros, I.; Downie, A.; Joseph, S. Agronomic values of
424 greenwaste biochar as a soil amendment. *Soil Res.* **2007**, *45* (8), 629–634; DOI:
425 10.1071/SR07109.
426 15. Steinbeiss, S.; Gleixner, G.; Antonietti, M. Effect of biochar amendment on soil carbon
427 balance and soil microbial activity. *Soil Biol. Biochem.* **2009**, *41* (6), 1301–1310; DOI:
428 10.1016/j.soilbio.2009.03.016.
429 16. Novak, J. M.; Busscher, W. J.; Laird, D. L.; Ahmedna, M.; Watts, D. W.; Niandou, M. A. S.
430 Impact of Biochar Amendment on Fertility of a Southeastern Coastal Plain Soil. *Soil Sci.*
431 **2009**, *174* (2), 105-112; DOI: 10.1097/SS.0b013e3181981d9a.
432 17. Zimmerman, A. R.; Gao, B.; Ahn, M.-Y. Positive and negative carbon mineralization
433 priming effects among a variety of biochar-amended soils. *Soil Biol. Biochem.* **2011**, *43* (6),
434 1169-1179; DOI: 10.1016/j.soilbio.2011.02.005.
435 18. McClellan, T.; Deenik, J.; Uehara, G.; Antal, M. Effects of flashed carbonized macadamia
436 nutshell charcoal on plant growth and soil chemical properties. *Am. Chem. Soc. Agron.*
437 *Abstr.* **2007**.
438 19. McLaughlin, H.; Anderson, P. S.; Shields F. E.; Reed, T. B. All biochars are not created
439 equal, and how to tell them apart. *Proceedings, North American Biochar Conference,*
440 *Boulder, Colorado,* **2009**, www.biochar-international.org/sites/default/files/All-Biochars--
441 Version2--Oct2009.pdf
442 20. McBeath, A. V.; Smernik, R. J. Variation in the degree of aromatic condensation of chars.
443 *Org. Geochem*. **2009**, *40* (12), 1161-1168; DOI: 10.1016/j.orggeochem.2009.09.006.
444 21. Cao, X.; Harris, W. Properties of dairy-manure-derived biochar pertinent to its potential use
445 in remediation. *Bioresource Technol.* **2010**, *101* (14), 5222-5228;
446 DOI: 10.1016/j.biortech.2010.02.052.

447 22. Knicker, H. Pyrogenic organic matter in soil: its origin and occurrence, its chemistry and
448 survival in soil environments. *Quatern, Int.* **2011**, *243* (2), 251-263; DOI:
449 10.1016/j.quaint.2011.02.037.
450 23. Schimmelpfennig, S.; Glaser, B. One step forward toward characterization: Some important
451 material properties to distinguish biochars. *J. Environ. Quality* **2012**, *41*, 1001-1013; DOI:
452 10.2134/jeq2011.0146.
453 24. Wiedner, K.; Naisse, C.; Rumpel, C.; Pozzi, A.; Wieczorek, P.; Glaser, B. Chemical
454 modification of biomass residues during hydrothermal carbonization – What makes the
455 difference, temperature or feedstock*? Org. Geochem.* **2013**, *54*, 91-100; DOI:
456 10.1016/j.orggeochem.2012.10.006.
457 25. Zhao, L.; Cao, X.; Mašek, O.; Zimmerman, A. Heterogeneity of biochar properties as a
458 function of feedstock sources and production temperatures. *J. Hazard. Mater.* **2013**, *256-*
459 *257*, 1-9; DOI:10.1016/j.jhazmat.2013.04.015.
460 26. Conte, P.; Marsala, V.; De Pasquale, C.; Bubici, S.; Valagussa, M.; Pozzi, A.; Alonzo, G.
461 Nature of water-biochar interface interactions. *GCB Bioenergy* **2013**, *5* (2), 116–121; DOI:
462 10.1111/gcbb.12009.
463 27. Sing, K. The use of nitrogen adsorption for the characterization of porous materials. *Colloid.*
464 *Surface. A.* **2001**, *187-188*, 3-9; DOI: 10.1016/S0927-7757(01)00612-4.
465 28. Dunn, K. J.; Bergman D. J.; Latorraca G. A. *Handbook of geographic exploration-seismic*
466 *exploration: Nuclear Magnetic Resonance Petrophysical and Logging Applications*;
467 Elsevier Science Ltd: Oxford, U.K., 2002.
468 29. Conte, P.; Alonzo, G. Environmental NMR: Fast-field-cycling Relaxometry, *eMagRes*,
469 **2013**, 389–398; DOI 10.1002/9780470034590.emrstm1330.
470 30. Kimmich, R.; Anoardo, E. Field-cycling NMR relaxometry. *Prog. Nucl. Mag. Res. Sp.*
471 **2004**, *44*, 257–320; DOI: 10.1016/j.pnmrs.2004.03.002.

31. Morozova-Roche, L. A.; Jones, J. A.; Noppe, W.; Dobson, C. M. Independent Nucleation and Heterogeneous Assembly of Structure during Folding of Equine Lysozyme. *J. Mol. Biol.* **1999**, *289* (4), 1055-1073; DOI: 10.1006/jmbi.1999.2741.
32. Borgia, G. C.; Brown, R. J. S.; Fantazzini, P. Uniform-Penalty Inversion of Multiexponential Decay Data. *J. Magn. Reson.* **1998**, *132* (1), 65-77; DOI: 10.1006/jmre.1998.1387.
33. Borgia, G. C.; Brown R. J. S.; Fantazzini, P. Uniform-Penalty Inversion of Multiexponential Decay Data: II. Data Spacing, $T_2$ Data, Systematic Data Errors, and Diagnostics. *J. Magn. Reson.* **2000**, *147* (2), 273-285; DOI: 10.1006/jmre.2000.2197.
34. Almendros, G.; Martinez, A. T.; Gonzalez, A. E.; Gonzalez-Vila F. J.; Fruend, R.; Luedemann, H.-D. CPMAS $^{13}C$ NMR study of lignin preparations from wheat straw transformed by five lignocellulose-degrading fungi. *J. Agric. Food Chem.* **1992**, *40* (7), 1297-1302; DOI: 10.1021/jf00019a043.
35. Callaghan, P. T.; Coy, A. PGSE NMR and molecular translational motion in porous media. In *Nuclear magnetic resonance probes of molecula dynamics*; Tycho, R., Ed.; Kluwer Academic Publishers: Dordrecht NL 1994; pp. 551.
36. Godward, J.; Gunning, P.; Hills, B.P. An NMR protocol for determining ice crystal size distributions during freezing and pore size distributions during freeze-drying. *Appl. Magn. Reson.* **1999**, *17* (4), 537-556; DOI: 10.1007/BF03162085.
37. Browenstein, K. R.; Tarr, C. E. Importance of classical diffusion in NMR studies of water in biological cells. *Phys. Rew. A* **1979**, *19* (6), 2446-2454; DOI: 10.1103/PhysRevA.19.2446.
38. Laudicina, V. A.; De Pasquale, C.; Conte, P.; Badalucco, L.; Alonzo, G.; Palazzolo, E. Effects of afforestation with four unmixed plant species on the soil–water interactions in a semiarid Mediterranean region (Sicily, Italy). *J. Soil Sediment* **2012**, *12* (8), 1222–1230; DOI 10.1007/s11368-012-0522-0.

497 39. Stingaciu, L. R.; Pohlmeier, A.; Blümler, P.; Weihermüller, L.; van Dusschoten, D.; Stapf,
498 S.; Vereecken, H. Characterization of unsaturated porous media by high-field and low-field
499 NMR relaxometry, *Water Resour. Res.* **2009,** *45* (8), DOI:10.1029/2008WR007459.
500 40. Korb, J.-P. Surface diffusion of liquids in disordered nanopores and materials: a field
501 cycling relaxometry approach. In *Fluid transport in nanoporous materials;* Conner W. C.;
502 Fraissard J., Eds.; Academic Press: Springer, NL, 2006.
503 41. Bakhmutov, V. I. Front Matter. In *Practical NMR relaxation for chemists*; John Wiley &
504 Sons, Ltd: Chichester, U.K., 2004.
505

506 **Figure captions**

507 **Figure 1.** CP-TOSS $^{13}C$ NMR spectra of poplar hydrochar (**A**) and pyrochar (**B**)

508 **Figure 2.** Relaxograms of poplar hydrochar (**A**) and pyrochar (**B**) acquired at the proton
509 Larmor frequency of 40 MHz

510 **Figure 3.** NMRD profiles of poplar hydrochar (**A**) and pyrochar (**B**)

511

512

513

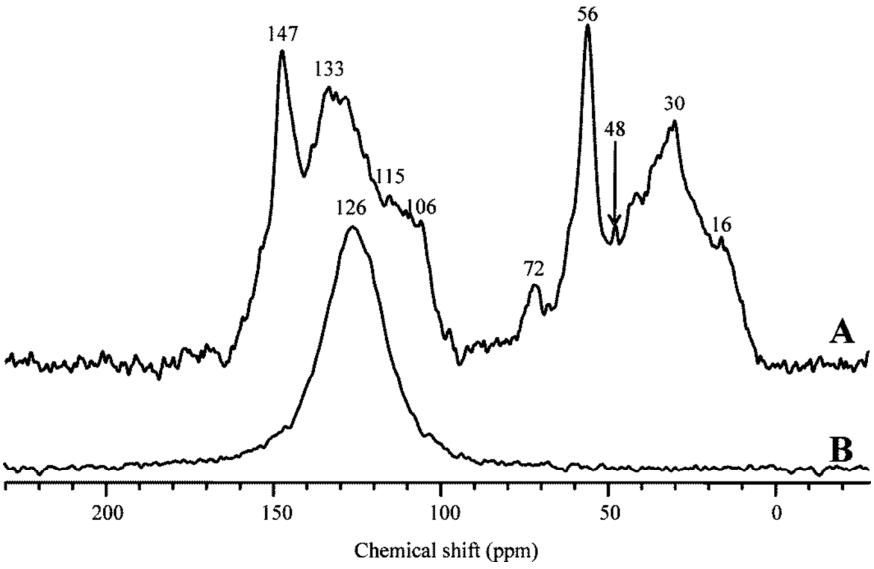


514

515 **Figure 1**

516

517

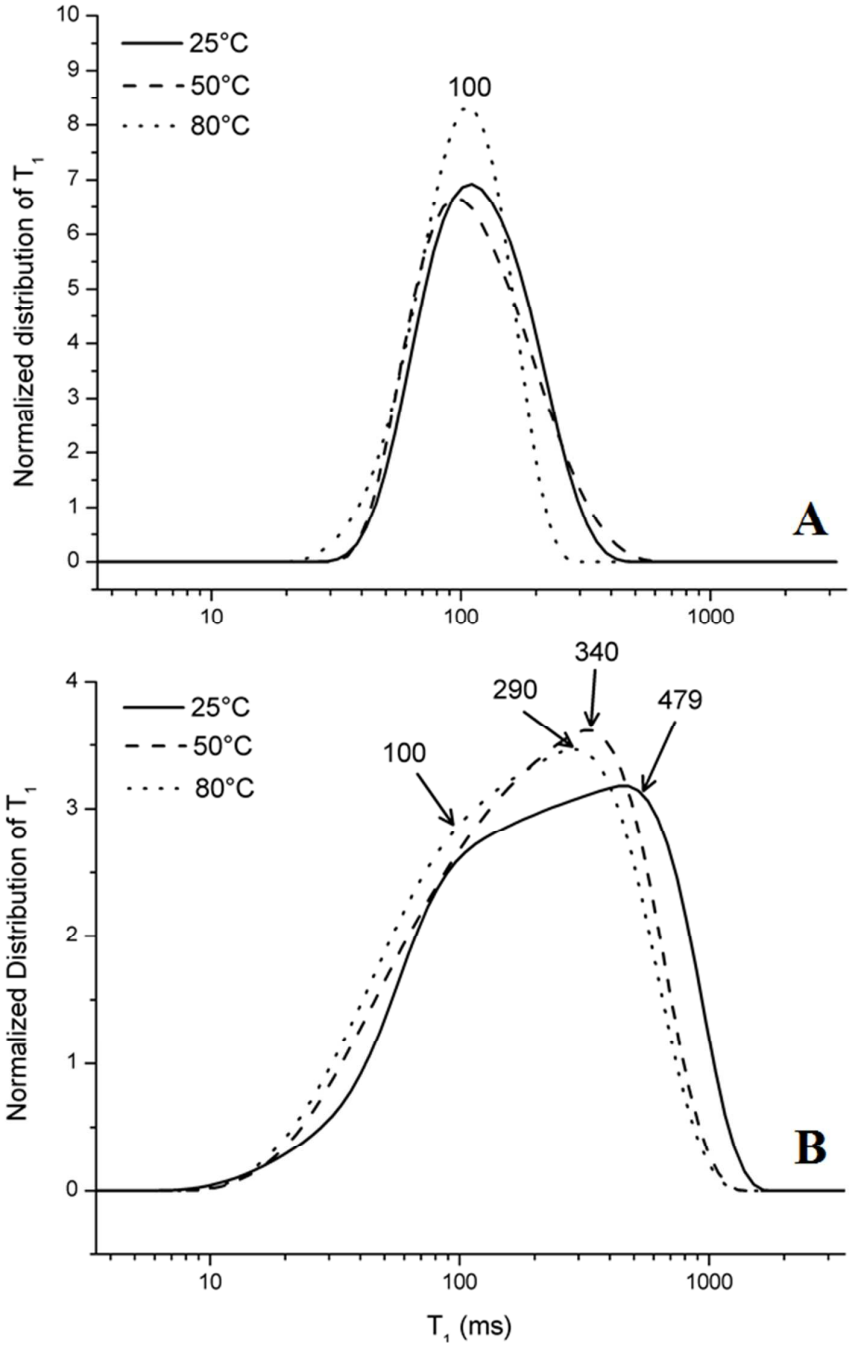


518

519 **Figure 2**

520

521

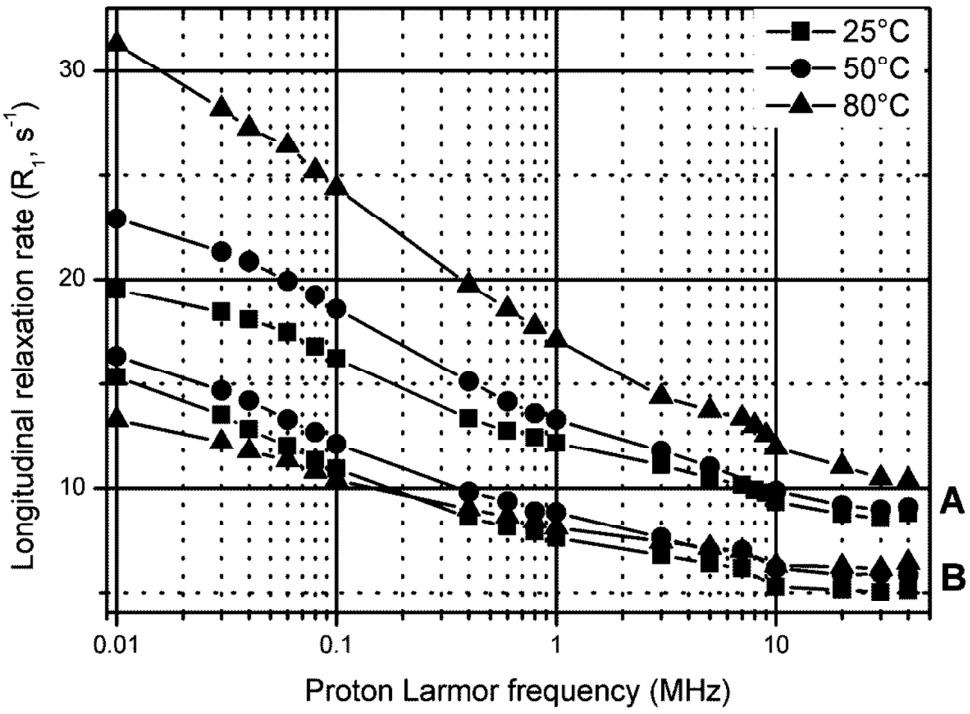


522

523 **Figure 3**

524

525 **Table of Contents/Abstract Graphic**

526

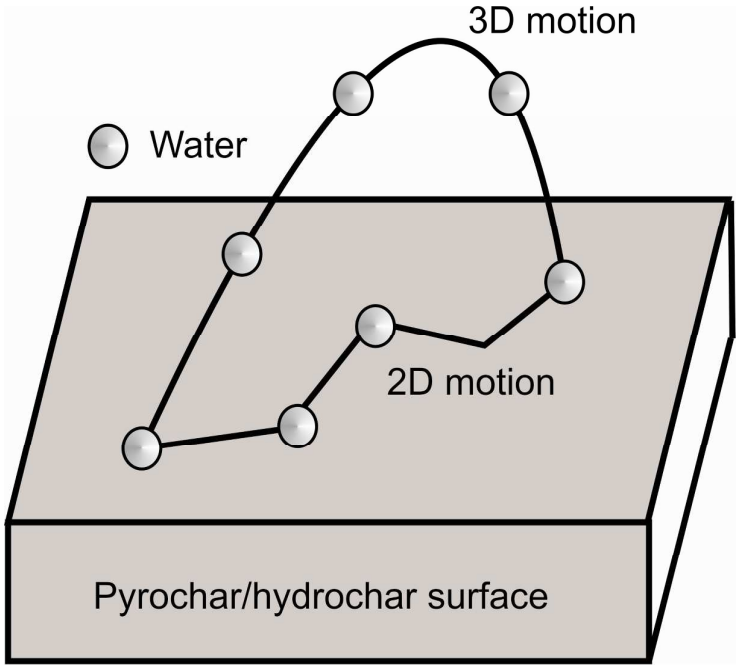


527